J. Fluid Mech. (1986), *vol.* 172, *pp.* 347–371
Printed in Great Britain

Evolution and decay of spherical and cylindrical N waves

By P. L. SACHDEV, V. G. TIKEKAR AND K. R. C. NAIR
Department of Applied Mathematics, Indian Institute of Science, Bangalore, India

(Received 4 January 1985 and in revised form 18 February 1986)

The Burgers equation, in spherical and cylindrical symmetries, is studied numerically using pseudospectral and implicit finite difference methods, starting from discontinuous initial (N wave) conditions. The study spans long and varied regimes – embryonic shock, Taylor shock, thick evolutionary shock, and (linear) old age. The initial steep-shock regime is covered by the more accurate pseudospectral approach, while the later smooth regime is conveniently handled by the (relatively inexpensive) implicit scheme. We also give some analytic results for both spherically and cylindrically symmetric cases. The analytic forms of the Reynolds number are found. These give results in close agreement with those found from the numerical solutions. The terminal (old age) solutions are also completely determined. Our analysis supplements that of Crighton & Scott (1979) who used a matched asymptotic approach. They found analytic solutions in the embryonic-shock and the Taylor-shock regions for all geometries, and in the evolutionary-shock region, leading to old age, for the spherically symmetric case. The numerical solution of Sachdev & Seebass (1973) is updated in a comprehensive manner; in particular, the embryonic-shock regime and the old-age solution missed by their study are given in detail. We also study numerically the non-planar equation in the form for which the viscous term has a variable coefficient. It is shown that the numerical methods used in the present study are sufficiently versatile to tackle initial-value problems for generalized Burgers equations.

1. Introduction

In the last two decades there has been widespread interest in nonlinear wave phenomena, mainly through the so-called 'model equations', derived from a larger system of PDEs, representing the most quintessential information from the parent system. Two of the most representative models are the Korteweg–de Vries equation and the Burgers equation. The former represents a balance between linear dispersion and quadratic nonlinearity, the latter between small linear diffusion and quadratic nonlinearity. The standard Burgers equation is written as

$$u_t + uu_x = \tfrac{1}{2}\delta u_{xx}, \tag{1.1}$$

(see Lighthill 1956) where, in the context of gasdynamics, $u = v + a - a_0$ is the excess wavelet velocity, v and a being the particle velocity and sound speed respectively; $x = \bar{x} - a_0 t$ is a coordinate measured in a frame of reference which moves in the same direction as the wave at the undisturbed speed of sound a_0; $\bar{x}$ and t are space and time coordinates. The coordinate x enables one to follow changes in the waveform without further changes in the origin. The coefficient δ is the 'diffusivity of sound', being a combination of different diffusivities which affect acoustic attenuation.

Equation (1.1) has a rich history (Benton & Platzman 1972), and its pre-eminence derives partly from its exact linearizability via the Hopf–Cole transformation into the standard heat equation. This enables one to solve pure initial-value problems for (1.1) by making use of the corresponding solutions for the heat equation in a simple and analytic manner (Lighthill 1956; Whitham 1974).

In physical applications, however, (1.1) is of limited use, since the model equations that represent reality are always more complicated than (1.1). Crighton (1979) has surveyed a host of generalized Burgers equations (GBEs) appearing in nonlinear acoustics. They include equations for unsteady finite-amplitude waves in gases, liquids and solids, bubble dynamics and cavitation in liquids, and phonon interactions and the quantum acoustics of solids. We choose here a particular generalized Burgers equation,

$$u_t + uu_x + \frac{Ju}{2t} = \tfrac{1}{2}\delta u_{xx}, \tag{1.2}$$

for a thorough treatment – both numerical and analytic. This equation combines the effects of geometrical spreading – spherical for $J = 2$ and cylindrical for $J = 1$ – with those of nonlinear convection and linear diffusion as represented by (1.1). Equation (1.2), with a sawtooth N wave initial condition which evolves and decays over an infinite time, poses as severe difficulties in analysis as any other generalized Burgers equation. The numerical methods we detail in this paper are sufficiently versatile and sturdy to handle related problems for other GBEs.

Equation (1.2) in a slightly different form (see (2.8)) was first mooted by Lighthill (1956). He argued that the geometrical effects or area change could be included in (1.1) by suitably redefining u and making δ in (1.1) a function of the area. To retain the analytic facility of the standard form of the Burgers equation, he approximated such an equation by assuming δ to be again a constant. This approximation would work if the shock remained thin and conformed to Taylor-shock structure. Both the assumptions fail as the N wave evolves, as we shall explain later in detail, (and as was first shown by Crighton & Scott 1979). Subsequently, Leibovich & Seebass (1974) derived (1.2), using the method of multiple scales. Since (1.2) (like most GBEs which arise directly from applications) does not admit linearization by a Hopf–Cole-like transformation, its exact solution for $J = 1$, 2 does not seem possible. Sachdev & Seebass (1973) studied (1.2) numerically using Douglas-Jones (1963) implicit finite difference scheme, starting with a smooth N wave with a Taylor-shock structure already embedded in it. Moreover, as Crighton (1979) pointed out, the calculations were stopped rather early in the evolution of the N wave. Thus, the embryonic-shock regime, when the sawtooth adjusts itself to a Taylor shock, and the evolution to final decay of the N wave, to its 'old age' when a purely linear form prevails, were missed in the numerical study. An important result of this study was, however, the derivation of approximate formulae for the lobe Reynolds number,

$$R = \frac{1}{\delta}\int_0^\infty u\,\mathrm{d}x,$$

which is the ratio of the product of velocity amplitude and lengthscale of the front lobe of the N wave to the diffusivity δ, for $J = 1, 2$. This was based on the assumption that the slope of the N wave at the node is given by the inviscid (lossless) solution for all time. The results thus obtained agreed very well with the numerical solutions, particularly for the spherical case. But this agreement was rather limited since the numerical study was not carried far enough in time. We shall show in the present paper that these formulae fail in the later near-linear or linear regimes of the wave.

As a sequel to the work of Sachdev & Seebass (1973), Crighton & Scott (1979) undertook a systematic matched asymptotic analysis of the N wave. They were able to find solutions in the embryonic-shock regime, and the shock wave displacement due to diffusion for all the three cases, $J = 0$, 1, and 2; for $J = 0$ the latter agreed with Lighthill's earlier derivation. Their analysis for this asymptotic solution was based on the following assumptions:

(i) the shock width remains small compared with the lengthscale of the lossless flow;

(ii) the shock displacement due to diffusivity remains small;

(iii) the Taylor shock retains its form.

These assumptions are violated in different order at later times, depending upon the geometry – plane, cylindrical or spherical. The main achievement of this work, besides finding the location of the centre of the shock for all geometries, was a careful delineation of various domains (in space and time) wherein different types of solutions are valid. For example, the perturbation solution for the plane case becomes invalid due to the failure of assumptions (ii) and (iii). For the cylindrical case, assumptions (i)–(iii) are all violated at the same time. For the spherical symmetry, the solution was obtained except for one small space–time region. The old-age time domain was demarcated and the old-age solution was completely predicted. The cylindrical case remained less complete; the magnitude of the multiplicative numerical amplitude constant in this case, in contrast to the spherical case, could not be determined.

The present paper constitutes a thorough revision of the work of Sachdev & Seebass (1973) in the light of the work of Crighton & Scott (1979). It gives a complete numerical study of non-planar N waves. Although the major thrust is numerical, there are also some analytical points, particularly for the cylindrical case, wherein we have been able to get a 'generalized similarity' form of the solution for a certain 'scaled inverse function', motivated by the known analytic form for the plane case. Thus, it complements the work of Crighton & Scott (1979), although the approaches are quite different. In the present paper, we use a pseudospectral finite difference approach for GBEs in a manner similar to that of Fornberg & Whitham (1978) for nonlinear dispersive waves (see also Gazdag & Canosa 1974 and Gazdag 1973). The use of this technique was necessitated by the inability of the Douglas–Jones implicit difference scheme to give accurate results for the (embryonic) shock regime when the initial profile is taken as a (discontinuous) sawtooth, in contrast to the smooth initial profile used by Sachdev & Seebass. The results obtained by the implicit scheme are so inaccurate in the shock regime that they would vitiate the subsequent (infinitely long in time) evolution of the profile. However, once the embryonic shock adjusts itself to a Taylor shock (which it does pretty swiftly for all geometries), the implicit difference scheme can be resorted to, and it yields an accuracy comparable to that of the pseudospectral approach in about one-ninth of the computer time.

We carried out our numerical computations all the way from a discontinuous sawtooth profile via embryonic shock, Taylor shock and a wide (evolutionary) shock to the old-age solution. We carried out first a careful comparison of our numerical solution with the known exact solution for the plane case when the Reynolds number is large. The embryonic shock for the plane case settles down to a Taylor shock when the constant t_0 in the plane solution

$$u = \frac{x/t}{1 + (t/t_0)^{\frac{1}{2}} \exp(x^2/2\delta t)}, \tag{1.3}$$

$$t_0 = [\exp(R_i) - 1]^2 t_i, \tag{1.4}$$

'converges', and the exact solution (1.3) takes over. The R_i is the Reynolds number at t_i. For smaller Reynolds number, say $R = 3$, Sachdev & Seebass have demonstrated that the Douglas–Jones implicit scheme gives excellent results. As we mentioned earlier, the pseudospectral approach is used only in the time regime extending from the sawtooth stage to the formation of the Taylor shock.

We check numerical shock details for all geometries with the analytic formulae of Crighton & Scott (1979). We note that their formulae give a good representation of the shock centre for $t \leqslant 30$, the initial time t_i being of order unity. The shock width at this stage is already of the order of the initial (lobe) width of the wave. Our 'generalized similarity solution', for the scaled inverse function for the cylindrical case gives excellent Reynolds number prediction for all times greater than $t \approx 300$. The formula of Sachdev & Seebass for $J = 1$ gives a good representation of the Reynolds number up to $t \approx 100$. Therefore, there is a time regime $100 < t < 300$, for which no analytic form of the Reynolds number has been found. For the spherical case, our analytic approach does not uniquely prescribe the form of the solution. However, a certain 'reasonable' choice of the arbitrary function in the analysis provides an excellent Reynolds number prediction for all times from the Taylor-shock regime to its final decay. It becomes possible to get (numerically) the unknown constants in the old-age (dipole) solutions for $J = 1, 2$. The old-age solution, thus uniquely determined, agrees very well with the numerical solution in the entire profile in the linear evolutionary regime of the wave. The Reynolds number, which is very small at this stage, is accurately determined by the old-age formula and agrees very well with that computed from the numerical solution.

The scheme of the paper is as follows. Section 2 gives the basic equations and initial conditions for the non-planar Burgers equation in the forms used by Sachdev & Seebass (1973) and Crighton & Scott (1979), and the relation between the two forms. Section 3 details the numerical schemes – implicit finite difference and pseudo-spectral. Sections 4, 6 and 7 deal with plane, cylindrical and spherical cases, respectively. Section 5 analyses the generalized similarity solution for the scaled inverse function for $J = 1, 2$. Finally, the results and conclusions of the present study are given in §8.

2. Basic equations and initial conditions

We take up the study of the generalized Burgers equation

$$u_t + uu_x + \frac{Ju}{(2t)} = \tfrac{1}{2}\delta u_{xx}; \tag{2.1}$$

the symbols have already been explained in the introduction. Initially, at $t = t_i$, we take a sawtooth profile of half length d_0

$$u(x, t_i) = \begin{cases} x & \text{for } |x| < d_0, \\ 0 & \text{for } |x| > d_0. \end{cases} \tag{2.2}$$

This is the point when a steepening of a wave under the lossless equation [$\delta = 0$ in (2.1)] has resulted in discontinuous shock formation. The subsequent evolution of the sawtooth takes place under the competitive influences of nonlinear convection, small diffusion, and geometrical spreading when $J = 1$ or 2. Before we proceed to give the numerical scheme for (2.1)–(2.2) in §3, it is worth giving the formulation of Crighton & Scott (1979), since we shall be comparing their matched asymptotic solution in the

thin-shock region with our numerical results. They commence their study with the Leibovich & Seebass (1974) form of (2.1), given by

$$U_t + \tfrac{1}{2}(\gamma+1)\,UU_x + JU/2t = \tfrac{1}{2}\Delta U_{xx}, \tag{2.3}$$

which coincides with (2.1) if we write $u = \frac{1}{2}(\gamma+1)\,U$ and $\Delta = \delta$. The variables in (2.3) are all dimensional and γ is the adiabatic constant. An initial disturbance $u_0(x)$ at $t = t_1$ with a lengthscale d_0 and amplitude U_0 is assumed. The dimensional form of the initial sawtooth is taken to be

$$U(x, t_1) = \left\{ \begin{array}{ll} U_0 \dfrac{x}{d_0} & \text{for } |x| < d_0, \\ 0 & \text{for } |x| > d_0, \end{array} \right\} \tag{2.4}$$

as produced, for example, by a piston motion at $x_0 = t_1/a_0$ where x_0 is the distance from centre of symmetry. A certain transformation of the variables is brought about to change (2.3) into a non-dimensional Burgers form with a variable viscosity:

$$\overline{V} = \left(\frac{t}{t_1}\right)^{\frac{1}{2}J} \frac{U}{U_0}, \quad X = \frac{x}{d_0}, \tag{2.5}$$

$$T = \left\{ \begin{array}{ll} 1 + \dfrac{\frac{1}{2}(\gamma+1)\,U_0(t-t_1)}{d_0} & \text{if } J = 0, \\ 1 + \dfrac{(\gamma+1)\,U_0(t_1^{\frac{1}{2}} t^{\frac{1}{2}} - t_1)}{d_0} & \text{if } J = 1, \\ 1 + \frac{1}{2}(\gamma+1)\,(U_0 t_1/d_0) \ln (t/t_1) & \text{if } J = 2. \end{array} \right\} \tag{2.6}$$

The transformations (2.5)–(2.6) are motivated by the inviscid form of the solution of (2.3), namely

$$u = \tfrac{1}{2}(\gamma+1)\,U = \left\{ \begin{array}{ll} \dfrac{x}{t} & \text{for } J = 0, \\ \dfrac{x}{2t} & \text{for } J = 1, \\ \dfrac{x}{t \ln t} & \text{for } J = 2. \end{array} \right\} \tag{2.7}$$

The factor $\frac{1}{2}(\gamma+1)$ is also removed by (2.5)–(2.6) and the initial time is reduced to $T = 1$. The new form of (2.3) is

$$\overline{V}_T + \overline{V}\overline{V}_X = \epsilon g(T)\,\overline{V}_{XX}, \tag{2.8}$$

where

$$g(T) = 1, \tfrac{1}{2}(T + T_0 - 1), \exp\left(\frac{T}{T_0}\right), \tag{2.9}$$

for plane, cylindrical and spherical symmetry, respectively,

$$\overline{V}(X, 1) = \left\{ \begin{array}{ll} X & \text{for } |X| < 1, \\ 0 & \text{for } |X| > 1. \end{array} \right. \tag{2.10}$$

The expressions for T_0 and ϵ for different geometries are

$$\left. \begin{array}{ll} T_0 = \dfrac{\gamma+1}{d_0} U_0 t_1, \epsilon = \dfrac{\Delta}{(\gamma+1) U_0 d_0} & \text{for } J = 0, \\ T_0 = \dfrac{\gamma+1}{d_0} U_0 t_1, \epsilon = \dfrac{2\Delta}{(\gamma+1) U_0 d_0 T_0} & \text{for } J = 1, \\ T_0 = \dfrac{\gamma+1}{2d_0} U_0 t_1, \epsilon = \dfrac{\Delta \exp(-1/T_0)}{(\gamma+1) U_0 d_0} & \text{for } J = 2. \end{array} \right\} \tag{2.11}$$

When the geometric and convection effects are of comparable importance, T_0 is of order 1 and ϵ is small.

3. Pseudospectral and implicit finite-difference schemes

It was clearly established by Sachdev & Seebass (1973) that the Douglas–Jones implicit predictor–corrector method for nonlinear parabolic equations is quite adequate in describing the evolution of an N wave, provided the initial profile is smooth. Indeed the sawtooth was endowed with a Taylor structure and this formed the initial profile. But this is not appropriate, as we pointed out in the introduction, since we skip the embryonic-shock region in the process. The sharp discontinuity in the sawtooth is not tackled properly by the implicit scheme; hence the need for a more accurate difference scheme. Before we describe the pseudospectral approach, we briefly discuss the Douglas–Jones predictor–corrector implicit scheme for the nonlinear parabolic equation

$$u_{xx} = F(x, t, u, u_x, u_t). \tag{3.1}$$

According to this scheme, the discretised form of (3.1) is

$$\left.\begin{aligned} \Delta_x^2 u_{i,j+\frac{1}{2}} &= F[x_i, t_{j+\frac{1}{2}}, u_{i,j}, \delta_x u_{i,j}, (u_{i,j+\frac{1}{2}} - u_{i,j})/(\tfrac{1}{2}k)], \text{ (predictor)}, \\ \tfrac{1}{2}\Delta_x^2 (u_{i,j+1} + u_{i,j}) &= F[x_i, t_{j+\frac{1}{2}}, u_{i,j+\frac{1}{2}}, \tfrac{1}{2}\delta_x (u_{i,j+1} + u_{i,j}), (u_{i,j+1} - u_{i,j})/k], \text{ (corrector)}, \end{aligned}\right\} \tag{3.2}$$

where

$$\left.\begin{aligned} \Delta_x^2 u_{i,j} &= h^{-2}(u_{i+1,j} - 2u_{i,j} + u_{i-1,j}), \\ \delta_x u_{i,j} &= (2h)^{-1}(u_{i+1,j} - u_{i-1,j}), \\ u_{i,j} &= u(x_i, t_j), \quad x_i = ih, \quad t_j = jk. \end{aligned}\right\} \tag{3.3}$$

This difference scheme has a truncation error of $O(h^2 + k^2)$ where h and k are space and time mesh sizes, respectively. Douglas & Jones (1963) have demonstrated the convergence of the difference scheme (3.2)–(3.3) for (3.1). The details of how the scheme (3.2) was used for (2.1) are given in Sachdev & Seebass (1973). To circumvent the difficulties posed by a sharp discontinuity, we chose a numerical scheme which is referred to as pseudospectral. This was employed earlier by Fornberg & Whitham (1978) for nonlinear model equations for dispersive waves. They could tackle initial 'well' conditions, as well as positive and negative step conditions. In this numerical approach what is special is the computation of space derivatives with very high accuracy by finite Fourier transform method. [Gazdag 1973 refers to this as the accurate space derivative (ASD) method.] The accuracy is limited only by the ability with which a distribution can be defined on a finite set of mesh points. Gazdag (1973) has shown that for the inviscid Burgers equation, the amplitude and phase of the error in the Fourier components remain bounded. He has also considered the evolution of a plane step to a Taylor shock under the governance of the plane Burgers equation; the accuracy obtained by the method, at an advanced time level in terms of spatial derivatives, was found to be very high.

We consider the finite Fourier transform,

$$\bar{u}(k_j, t) = \frac{1}{K} \sum_{m=0}^{K-1} u(m\Delta x, t) \exp(-ik_j m\Delta x), \tag{3.4}$$

of a function $u(x, t)$ over the interval $(0, 2\pi)$ of x. Here, the mesh size Δx is equal to

$2\pi/K$, with K denoting the number of mesh points; k_j are the wavenumbers varying between 0 and $K-1$. The inverse finite Fourier transform is given by

$$u(m\,\Delta x, t) = \sum_{|k_j| < \frac{1}{2}K} \bar{u}(k_j, t) \exp(\mathrm{i} k_j m\,\Delta x). \tag{3.5}$$

The spatial derivatives easily follow from (3.5):

$$\left.\begin{aligned} u_x(m\,\Delta x, t) &= \sum_{|k_j| < \frac{1}{2}K} \mathrm{i} k_j \bar{u}(k_j, t) \exp(\mathrm{i} k_j m\Delta x), \\ u_{xx}(m\,\Delta x, t) &= \sum_{|k_j| < \frac{1}{2}K} (\mathrm{i} k_j)^2 \bar{u}(k_j, t) \exp(\mathrm{i} k_j m\Delta x). \end{aligned}\right\} \tag{3.6}$$

The solution at $t+\Delta t$ is obtained from the Taylor series

$$u(x, t+\Delta t) = u(x,t) + \Delta t u_t + \frac{\Delta t^2}{2!} u_{tt} + \frac{\Delta t^3}{3!} u_{ttt} + \ldots, \tag{3.7}$$

wherein the time derivatives u_t, u_{tt}, etc., are substituted from the basic equation (2.1) in terms of the spatial derivatives as follows:

$$\left.\begin{aligned} u_t &= -uu_x - \frac{Ju}{2t} + \tfrac{1}{2}\delta u_{xx}, \\ u_{tt} &= -u_t u_x - u\,u_{xt} - \frac{J}{2t} u_t + \frac{Ju}{2t^2} + \tfrac{1}{2}\delta u_{xxt}, \\ u_{ttt} &= -u_{tt} u_x - 2u_t u_{xt} - u\,u_{xtt} - \frac{J}{2t} u_{tt} + \frac{J}{t^2} u_t - \frac{Ju}{t^3} + \tfrac{1}{2}\delta u_{ttxx}. \end{aligned}\right\} \tag{3.8}$$

In our computations, we used four terms in the Taylor series (3.7), so that the truncation error is $O(\Delta t^4)$ (Gazdag 1973). The initial domain was taken to be $(0, 2\pi)$ and was divided into 256 equal mesh points in which the (initial) sawtooth profile $u = x$ in $|x| < d_0$ occupied only 80 points so as to allow the profile to grow due to diffusion as it evolves. We describe the actual calculations in the next section with reference to the plane Burgers equation, for which the exact solution is known.

4. The plane Burgers equation

In this section we present the numerical calculations for the plane Burgers equation and compare them with the exact solution. All computations discussed here were carried out with single precision on a microcomputer. Equation (2.1) with the discontinuous initial profile (2.2) was solved by the pseudospectral method (hereinafter to be referred to as the PS method) as detailed in §3. The spatial domain was normalized to $(0, 2\pi)$ to satisfy periodic conditions required by the finite Fourier transform. The initial sawtooth was placed in the middle of the domain with adequate space on either side of the wave to allow for its diffusion. We chose the mesh sizes as $\Delta x = 0.005$ and $\Delta t = 0.01$, and $d_0 = 0.205$, $u_0 = 0.205$, $\delta = 0.001$, $t_i = 1$. The initial number of mesh points was taken to be 256. As the computation commenced, we noticed a spurious tail of magnitude $O(10^{-3})$ in the first timestep and it was cut off. The tail in the subsequent calculations was much smaller and, in fact, vanished after a few steps. Similar spurious tails were noticed by Gazdag & Canosa (1974). First we checked the accuracy of the PS method. At each time level the constant t_0 as given by (1.4) was calculated. Table 1 shows the convergence of t_0 to a (definite) finite value at about $t = 2$.

This signalled the end of the embryonic-shock regime, whereafter the shock

t	R	$10^{-10}t_0$
1.0	21.354	0.18793
1.1	21.488	0.22534
1.2	21.446	0.22556
1.4	21.369	0.22564
1.6	21.302	0.22564
1.8	21.243	0.22563
2.0	21.190	0.22563

TABLE 1. 'Convergence' of the value of t_0 as time increases (see (1.4))

	$u(x, t = 15)$			Difference	
x	IMP	PS	Exact		
(1)	(2)	(3)	(4)	(2)−(4)	(3)−(4)
0.03	0.002	0.002	0.002	0	0
0.33	0.022	0.022	0.022	0	0
0.63	0.04196	0.04196	0.04196	0	0
0.72	0.04562	0.04550	0.04550	0.00012	0
0.75	0.04049	0.04037	0.04037	0.00012	0
0.78	0.02453	0.02474	0.02474	0.00021	0
0.81	0.00833	0.00843	0.00843	−0.00010	0
0.84	0.00194	0.00192	0.00192	0.00002	0
0.87	0.00038	0.00037	0.00037	0.00001	0
0.90	0.00007	0.00007	0.00007	0	0

TABLE 2. Comparison of numerical (IMP and PS) solution with exact solutions of the Burgers equation

assumes the form of a Taylor shock. Table 2 shows that the numerical solution (PS) agrees with the exact solution to more than five decimal places. At about $t = 6$ the Taylor shock widened to about $\frac{1}{4}d_0$. At this stage we switched over to the implicit predictor–corrector scheme (hereinafter to be called the IMP method), as the PS method is too expensive in terms of computer time to be used throughout the evolution and as the accuracy of the IMP method is reasonably good (with an error of $O(10^{-4})$ in the worst case in the shock regime). This is clear from table 2 which shows the solution of (2.1) at $t = 15$ (the initial profile for the IMP scheme was the smoothed out solution at $t = 14$). The last two columns give the difference between IMP and the exact solution, and PS and the exact solution. In the early stage, at $t = 3$, the IMP method had an error $O(9 \times 10^{-4})$ in the shock layer while the PS method had an error $O(3 \times 10^{-5})$. As the profile became smoother at $t=6$, the error by the PS scheme reduced to $O(10^{-6})$ while the IMP method still has an error $O(3 \times 10^{-4})$ in the shock layer and a smaller error $O(10^{-6})$ elsewhere. This error in the shock transition is characteristic of the IMP method, and it persists throughout the calculation when the Reynolds number is large, but does not grow, as evidenced by the solutions at later times. Table 3 gives the numerical (IMP) and the exact solutions in the large-Reynolds-number regime for the plane Burgers equation at $t = 200$, 400 and 500. For smaller initial Reynolds numbers, say $R = 3$, and with a smooth initial shock, the solution obtained by Sachdev & Seebass (hereinafter referred to as SS) shows the same order of accuracy. With a reduced mesh size there is a uniform

$u(x, 200)$			$u(x, 400)$			$u(x, 500)$		
x	Num.	Exact	x	Num.	Exact	x	Num.	Exact
0.04	0.00020	0.00020	0.08	0.00020	0.00020	0.08	0.00016	0.00016
0.24	0.00120	0.00120	0.88	0.00220	0.00220	1.68	0.00330	0.00336
0.84	0.00420	0.00420	2.48	0.00620	0.00620	3.28	0.00644	0.00656
1.84	0.00920	0.00920	3.44	0.00847	0.008402	3.92	0.00743	0.00749
2.48	0.01211	0.01204	3.52	0.00851	0.008403	4.08	0.00695	0.00699
2.64	0.01080	0.01072	3.60	0.00835	0.00821	4.48	0.00133	0.00145
2.84	0.00297	0.00310	4.08	0.00090	0.00096	4.88	0.00005	0.00005
3.04	0.00022	0.00022	4.48	0.00002	0.00002			
3.24	0.00001	0.00001						

TABLE 3. Numerical (IMP) and exact solutions of the Burgers equation

$u(x, t = 3)$					
x (1)	IMP $\Delta x = 0.01$ (2)	IMP $\Delta x = 0.005$ (3)	PS $\Delta x = 0.01$ (4)	PS $\Delta x = 0.005$ (5)	Exact (6)
0.01	0.0033334	0.0033334	0.003333	0.0033334	0.0033333
0.05	0.0166670	0.0166670	0.0166678	0.0166669	0.0166667
0.09	0.0300006	0.0300006	0.0300021	0.0300005	0.03
0.13	0.0433342	0.0433343	0.0433365	0.0433341	0.0433333
0.17	0.0566678	0.0566679	0.0566710	0.0566677	0.0566667
0.21	0.0700015	0.0700016	0.0700057	0.0700013	0.0699999
0.25	0.0833348	0.0833343	0.0833390	0.0833331	0.0833312
0.33	0.1084517	0.1047879	0.1039273	0.1039248	0.1039148
0.37	0.0144973	0.0163013	0.0170474	0.0170449	0.0170647
0.39	0.0016943	0.0016499	0.0016279	0.0016321	0.0016365

TABLE 4. Solution of plane Burgers equation using different mesh sizes and different methods. Initial profile at $t = 2$ was taken to be smooth.

improvement of accuracy in the entire profile by the PS method, whereas the IMP method shows little change in the shock regime (see table 4). As the profile evolved under the influence of diffusion and nonlinear convection, the non-zero part of the profile would occupy about 1200 mesh points when $t = 100$. During the evolutionary process we restricted the number of mesh points to 256 by doubling the mesh size whenever it became necessary. In the plane case the exact solution was always available for comparison (see table 3).

We also examined the evolution of the initial discontinuous profile using the IMP method, starting at $t = 1$. It was observed that the error in the numerical solution is $O(10^{-3})$ at the grid point. Further, t_0 given by (1.4) did not converge but continued to oscillate for a long time. The position of the shock centres, as given by Crighton & Scott (1979), is

$$s = d_0 T^{\frac{1}{2}}(1 - \epsilon \ln T), \tag{4.1}$$

and the numerical shock centre, following Lighthill (1956), was approximated by

$$s = \tfrac{1}{2}(x_1 + x_2), \tag{4.2}$$

t (1)	x_m (2)	u_m (3)	Shock width (4)	Shock centre Num. (5)	Shock centre CS (6)	Difference (5)−(6) (7)	u_d (8)	u_d/u_m (9)
1.1	0.2	0.180	0.020	0.218	0.217	0.001	0.027	0.151
1.3	0.216	0.162	0.027	0.238	0.238	0.0	0.014	0.088
1.5	0.232	0.150	0.033	0.254	0.258	−0.004	0.025	0.169
2.0	0.267	0.129	0.039	0.292	0.302	−0.01	0.04	0.309
3.0	0.324	0.105	0.045	0.358	0.373	−0.015	0.046	0.442
10.0	0.582	0.057	0.08	0.646	0.687	−0.041	0.034	0.601
20.0	0.81	0.04	0.114	0.906	0.969	−0.063	0.025	0.623
30.0	0.992	0.032	0.14	1.104	1.183	−0.079	0.021	0.638
50.0	1.273	0.025	0.18	1.415	1.521	−0.0106	0.016	0.644

TABLE 5. Shock details for plane Burgers' equation, $t_i = 1$, $\epsilon = 0.0099$ (see (2.11)). x_m = location of the point of maximum amplitude u_m, u_d = maximum of the difference, between Taylor-shock structure and numerical shock structure. CS, Crighton & Scott (1979)

t	R (num.)	R (exact)	$u_x(0,t)$ Num.	$u_x(0,t)$ Exact
2.0	21.19044	21.19044	0.50000	0.50000
5.0	20.73211	20.73230	0.20000	0.20000
10.0	20.38545	20.38572	0.10000	0.10000
20.0	20.03925	20.03915	0.05000	0.05000
50.0	19.58110	19.58100	0.02000	0.02000
100.0	19.23382	19.23444	0.01000	0.01000
200.0	18.88652	18.88785	0.00500	0.00500
300.0	18.68374	18.68512	0.00333	0.00333
400.0	18.53919	18.54127	0.00250	0.00250

TABLE 6. Reynolds number for plane Burgers equation at different times as obtained from numerical (IMP) and exact solutions. This table also gives $u_x(0,t)$

where x_1 and x_2 are spatial coordinates of the points having $u = 0.95u_m$ and $u = 0.05u_m$, respectively, u_m being the maximum amplitude of the wave. The position of the centre as given by both the formulae agrees for $t \leqslant 30$ to an error less than 7 % (see table 5). The shock width S defined by

$$S = x_2 - x_1, \tag{4.3}$$

is also given in table 5. The shock width at $t = 500$ is 2.9 times the initial (half) length of the wave profile. The maximum of the difference between the numerical shock structure and the Taylor-shock structure defined by

$$u = \frac{u_m}{1+\exp\left(u_m\,(x-s)/\delta\right)}, \tag{4.4}$$

is also given in table 5. In the large-Reynolds-number regime which we have depicted in table 5, the shock structure is essentially Taylor-type. The numerical and analytic values of the lobe Reynolds number and the slopes of the profile at the origin are given in table 6. The Reynolds number, analytic and numerical, agrees to 5

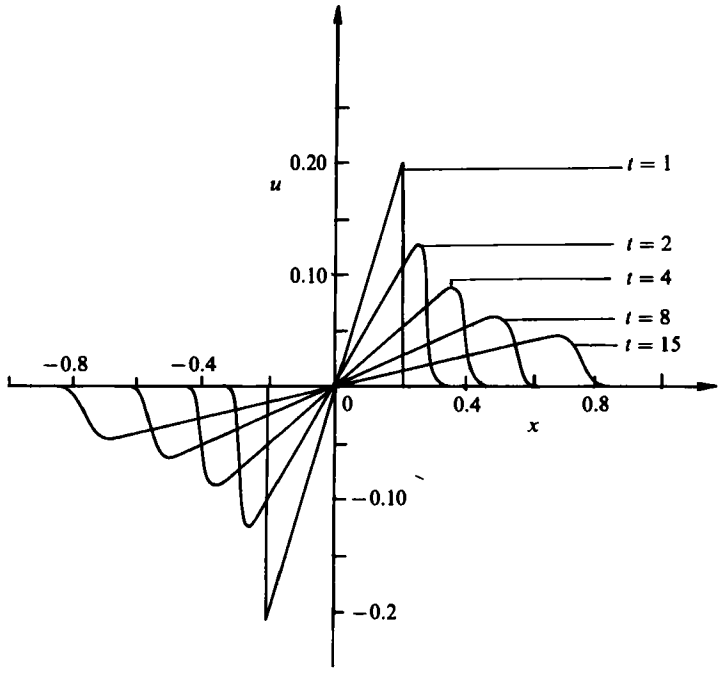

FIGURE 1. Solution of plane Burgers equation: embryo shock to Taylor shock.

significant digits whereas the slope at the origin agrees with the slope from the inviscid formula [cf. (2.7)] extremely well, confirming the observation of SS in this regard.

The wave profile in the plane case decays very slowly. In fact, the lobe Reynolds number changes from 21 at $t = 1$ to 18.1 at $t = 500$. While the amplitude of the wave falls considerably from $u_m = 0.2$ at $t = 1$ to $u_m = 0.007$ at $t = 500$, the profile diffuses to 28 times its original length. This explains the small change in the Reynolds number. Sachdev & Seebass (1973) have previously confirmed the accuracy of the IMP scheme in the smaller-Reynolds-number regime, $R = 3$ (see table 2 in SS).

The diffusion of the plane N wave is shown in figures 1 and 2.

5. An analytic approach

Before we present the numerical results, we derive a 'generalized similarity solution', in a form similar to that for the plane case, for a function which is a certain 'scaled' inverse of u. It is well known that the similarity solution which exists for the cylindrical case is not relevant to the present problem (Sinai 1976). The following analysis applies to all geometries, $J = 0, 1, 2$. Equation (2.1) is transformed by introducing the variables

$$v = \frac{u}{(2\delta)^{\frac{1}{2}}}, \quad \tau = t^{\frac{1}{2}}, \quad \xi = \frac{x}{(2\delta t)^{\frac{1}{2}}}, \tag{5.1}$$

into

$$\tau v_\tau + (2\tau v - \xi) v_\xi + Jv = \tfrac{1}{2} v_{\xi\xi}. \tag{5.2}$$

Another change of variables

$$\eta = \xi^2, \quad V = \eta^{\frac{1}{2}} v^{-1}, \tag{5.3}$$

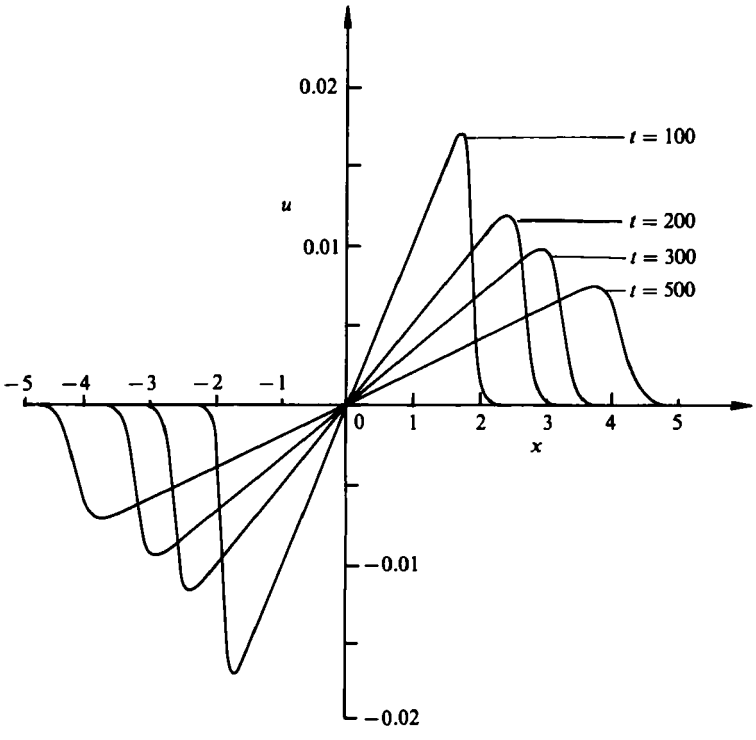

FIGURE 2. Solution of plane Burgers equation: thick-shock regime.

transforms (5.2) into

$$2\eta V V_{\eta\eta} - 4\eta V_\eta^2 + (2\tau - V)(V - 2\eta V_\eta) + V(JV - \tau V_\tau) + 3VV_\eta = 0. \tag{5.4}$$

In terms of the variables V, τ and η, the N wave solution (1.3) for the plane Burgers equation becomes

$$\begin{aligned} V &= \tau + t_0^{-\frac{1}{2}}\tau^2 e^\eta, \\ &= \tau + t_0^{-\frac{1}{2}}\tau^2 + t_0^{-\frac{1}{2}}\tau^2\eta + \frac{t_0^{-\frac{1}{2}}\tau^2\eta^2}{2!} + \ldots. \end{aligned} \tag{5.5}$$

Indeed, the transformations (5.1) and (5.3) were motivated by the form (1.3). Now we seek solution of (5.4) for $J = 1, 2$ in the form

$$V = \sum_{i=0}^{\infty} f_i(\tau)\,\eta^i/i!, \tag{5.6}$$

[cf. (5.5)]. Substituting (5.6) into (5.4) and equating coefficients of $\eta^0, \eta^1, \eta^2, \ldots$, on both sides, we get

$$3f_1 + (J-1)f_0 - \tau f_0' + 2\tau = 0, \tag{5.7}$$

$$5f_0 f_2 - f_1(f_1 - 2Jf_0 + 2\tau) - \tau(f_1 f_0' + f_0 f_1') = 0, \tag{5.8}$$

$$7f_0 f_3 - f_2[3f_1 - 2(J+1)f_0 + \tau f_0' + 6\tau] - \tau f_0 f_2' + 2f_1[(J+1)f_1 - \tau f_1'] = 0, \tag{5.9}$$

etc. We consider the cases $J = 1, 2$ separately.

(i) $J = 1$. We choose f_0, f_1, f_2 in the form

$$f_0 = 2\tau + b_2\tau^2 + b_3\tau^3, \tag{5.10}$$

$$f_1 = c_1\tau + c_2\tau^2 + c_3\tau^3, \tag{5.11}$$

and

$$f_2 = d_1\tau + d_2\tau^2 + d_3\tau^3, \tag{5.12}$$

by combining suitably the explicit time dependences in the inviscid and the asymptotic forms (2.7) and (5.14) for the solution to (1.2). Thus, (5.10)–(5.12) are dictated by the known behaviour of this solution. It turns out that in this case all the coefficients $b_2, c_1, c_2, c_3, d_1, d_2$ and d_3 become known in terms of b_3 (which in any case should remain unknown since it is the coefficient in the asymptotic behaviour which generally cannot be found except numerically; cf. the appearance of $t_0^{-\frac{1}{2}}$ in the planar solution). The coefficients are explicitly found to be $c_1 = d_1 = 0$, $c_2 = \frac{2}{3}b_2, d_2 = \frac{4}{15}b_2, c_3 = d_3 = b_3$ and $b_2 = +3b_3^{\frac{1}{3}}$ or $-3b_3^{\frac{1}{3}}$. The choice $b_2 = +3b_3^{\frac{1}{3}}$ turns out to be the appropriate one. The other functions, $f_i, i > 2$, become known without solving the differential equation. This is not entirely unexpected. It does happen in many problems (see Canosa 1973, for example). The $f_i, i > 2$, are rational functions of τ having correct asymptotic behaviour for $\tau \to \infty$. For example,

$$f_3 = \frac{\frac{16}{105}b_2\tau^2 + \frac{54}{35}b_3\tau^3 + \frac{27}{35}b_2b_3\tau^4 + b_3^2\tau^5}{2 + b_2\tau + b_3\tau^2}, \tag{5.13}$$

$$\sim b_3\tau^3 \quad \text{as } \tau \to \infty.$$

This agrees with the asymptotic 'old-age' form

$$u = C_1 x t^{-2} \exp\left(-\frac{x^2}{2\delta t}\right), \tag{5.14}$$

when the transformation (5.1) and (5.3), etc., are carried out. The cylindrical N-wave solution may therefore be written as

$$u = xt^{-\frac{1}{2}}[f_0(t) + \xi f_1(t) + \frac{\xi^2}{2!}f_2(t) + \ldots]^{-1}, \tag{5.15}$$

where $f_0(t), f_1(t), f_2(t)$ etc. are given by (5.10)–(5.12) with $\tau = t^{\frac{1}{2}}$ and $\xi = x(2\delta t)^{-\frac{1}{2}}$. To obtain the lobe Reynolds number, we integrate (1.2) with $J = 1$ from $x = 0$ to $x = \infty$, and use the condition that u and u_x vanish at $x = \infty$. $u_x(0, t)$ is found from (5.15) to be

$$u_x(0, t) = \frac{1}{t^{\frac{1}{2}}}[2t^{\frac{1}{2}} + 3b_3^{\frac{1}{3}}t + b_3t^{\frac{3}{2}}]^{-1}. \tag{5.16}$$

We thus have

$$\frac{\mathrm{d}R}{\mathrm{d}t} + \frac{R}{2t} = -\frac{1}{2t^{\frac{1}{2}}}[2t^{\frac{1}{2}} + 3b_3^{\frac{1}{3}}t + b_3t^{\frac{3}{2}}]^{-1}. \tag{5.17}$$

Integration of (5.17) gives

$$R = \left(\frac{C}{t}\right)^{\frac{1}{2}} + (tb_3)^{-\frac{1}{2}} \ln\left[\frac{t^{\frac{1}{2}} + 2b_3^{-\frac{1}{2}}}{t^{\frac{1}{2}} + b_3^{-\frac{1}{2}}}\right], \tag{5.18}$$

where C is the constant of integration.

(ii) $J = 2$. In this case, the equations for $f_0, f_1, \ldots$, are found to be

$$3f_1 + f_0 - \tau f_0' + 2\tau = 0, \tag{5.19}$$

$$5f_0f_2 - f_1(f_1 - 4f_0 + 2\tau) - \tau(f_1f_0' + f_0f_1') = 0 \quad \text{etc.}, \tag{5.20}$$

From (5.19) and (5.20), and the inviscid solution (2.6) for $J = 2$, it seems natural to introduce the variables

$$f_0 = \tau F_0, \quad f_1 = \tau F_1, \quad f_2 = \tau F_2, \quad \ldots. \tag{5.21}$$

and

$$\theta = \ln \tau.$$

Equations (5.19) and (5.20) become

$$\frac{\mathrm{d}F_0}{\mathrm{d}\theta} = 3F_1 + 2, \tag{5.22}$$

$$F_0 \frac{\mathrm{d}F_1}{\mathrm{d}\theta} = F_1\left(2F_0 - \frac{\mathrm{d}F_0}{\mathrm{d}\theta} - F_1 - 2\right) + 2F_0 F_2, \quad \text{etc.} \tag{5.23}$$

Unlike the case $J = 1$, it does not seem possible to get F_0 explicitly. Indeed, it can be verified that F_1, F_2 etc. can be uniquely determined once F_0 is prescribed. There seems no unique logical way to fix F_0. However, we have found that a linear combination of the terms contributing to f_0 from the inviscid solution and the 'old age' asymptotic solution gives good results (see §7). Thus, taking

$$u = x\left[f_0(t) + \xi f_1(t) + \frac{\xi^2 f_2(t)}{2!} + \ldots\right]^{-1}, \tag{5.24}$$

where

$$f_0(t) = t \ln t + a_0 t^{\frac{1}{2}}, \tag{5.25}$$

we find, as for $J = 1$, that the Reynolds number is given by

$$R = \frac{\bar{C}}{t} - \frac{1}{2t}\int_{t_i}^{t} \frac{\mathrm{d}y}{\ln y + a_0 y^{\frac{1}{2}}}, \tag{5.26}$$

where $\bar{C}$ is the constant of integration.

6. The cylindrical Burgers equation

The initial discontinuous profile for this case was taken to be the inviscid solution,

$$u(x, t_i) = \begin{Bmatrix} \dfrac{x}{2t_i} & \text{for } |x| < d_0, \\ 0 & \text{for } |x| > d_0, \end{Bmatrix} \tag{6.1}$$

where $t_i = 0.5$, $d_0 = 0.205$ and $R(t_i) = 21.0125$. The transition of this profile to one with a Taylor shock, via the embryonic stage is shown in figure 3. The shock details, including the shock centre as given by Crighton & Scott (1979; hereinafter referred to as CS) are given in table 7. The shock centre, as given by the matched asymptotic solution of CS,

$$s = d_0 T^{\frac{1}{2}}[1 - \delta(T - 1 + (T_0 - 1)\ln T)/(\gamma + 1) U_0 d_0 T_0], \tag{6.2}$$

agrees with the numerical solution up to $t \approx 25$, with an error less than 5%. At this stage, the shock width is approximately $1.4d_0$. The shock is rather thick and one of the assumptions underlying this stage of the matched asymptotic solution of CS breaks down. The maximum of the difference in the amplitude of numerical shock and the Taylor shock as a fraction of u_m increases as the shock thickens. The computations were carried from $t = 0.5$ to $t = 2000$. Figures 3–5 show the evolution of the wave in three typical time regimes – Taylor shock, thick shock and old age. The Reynolds numbers – numerical, analytic according to (5.18), and by the formula of SS – are shown in table 8. This table also shows the numerical value of the slope

t (1)	x_m (2)	u_m (3)	Shock width (4)	Shock centre Num. (5)	Shock centre CS (6)	Difference (5)−(6) (7)	u_d (8)	u_d/u_m (9)
1.0	0.221	0.108	0.035	0.249	0.250	−0.001	0.013	0.118
2.0	0.255	0.061	0.057	0.297	0.301	−0.004	0.011	0.176
3.0	0.275	0.044	0.073	0.330	0.334	−0.004	0.008	0.182
4.0	0.291	0.034	0.087	0.355	0.359	−0.004	0.006	0.184
5.0	0.305	0.028	0.1	0.377	0.380	−0.003	0.005	0.184
6.0	0.314	0.024	0.113	0.395	0.397	−0.002	0.004	0.184
7.0	0.323	0.021	0.125	0.411	0.412	−0.001	0.004	0.185
8.0	0.330	0.019	0.135	0.426	0.426	0.0	0.004	0.185
9.0	0.337	0.017	0.145	0.440	0.438	0.002	0.003	0.186
10.0	0.343	0.015	0.154	0.452	0.449	0.003	0.003	0.197
15.0	0.368	0.011	0.196	0.506	0.493	0.013	0.003	0.239
20.0	0.387	0.008	0.232	0.548	0.526	0.022	0.002	0.267
30.0	0.414	0.006	0.293	0.615	0.575	0.041	0.002	0.311
40.0	0.436	0.004	0.346	0.670	0.610	0.059	0.001	0.341
50.0	0.437	0.003	0.391	0.717	0.639	0.079	0.001	0.354
100.0	0.521	0.002	0.570	0.898	0.762	0.171	0.001	0.412
150.0	0.573	0.001	0.705	1.03	0.775	0.26	0.0004	0.427

TABLE 7. Shock details for cylindrical Burgers equation, $T_0 = 1.2$, $\epsilon = 0.0165$ (see (2.11)); abbreviations are explained in table 5.

t	R(Num)	R Equation (6.3)	R Equation (5.18)	$u_x(0,t)$ Num.	$u_x(0,t)$ Analytic
5.0	6.52471	6.52365	5.61662	0.10039	0.10000
10.0	4.46658	4.46647	3.84512	0.05014	0.05000
20.0	3.01153	3.01183	2.59951	0.02502	0.02500
50.0	1.72225	1.72107	1.50794	0.00976	0.01000
100.0	1.08011	1.07054	0.97085	0.00447	0.00500
150.0	0.80369	0.78234	0.73931	0.00269	0.00333
200.0	0.64448	0.61054	0.60448	0.00182	0.00250
250.0	0.53965	0.49329	0.51440	0.00132	0.00200
350.0	0.40882	0.33949	0.39940	0.00080	0.00143
450.0	0.32989	0.24036	0.32781	0.00053	0.00111
650.0	0.23854	0.11602	0.24178	0.00029	0.00077
850.0	0.18711	0.03869	0.19106	0.00018	0.00059
1050.0	0.15374	−0.01582	0.15726	0.00012	0.00048
1350.0	0.12160	−0.07255	0.12320	0.00008	0.00037
1650.0	0.10055	−0.11336	0.10024	0.00005	0.00030
2000.01	0.08364	−0.14882	0.08133	0.00004	0.00025

TABLE 8. Reynolds number for cylindrical Burgers equation at different times: numerical, and analytic according to (6.3) and (5.18) with $C^{\frac{1}{3}} = -4.716$, $b_3^{-\frac{1}{3}} = 26.44$. Numerical and analytic values of $u_x(0,t)$ are also shown

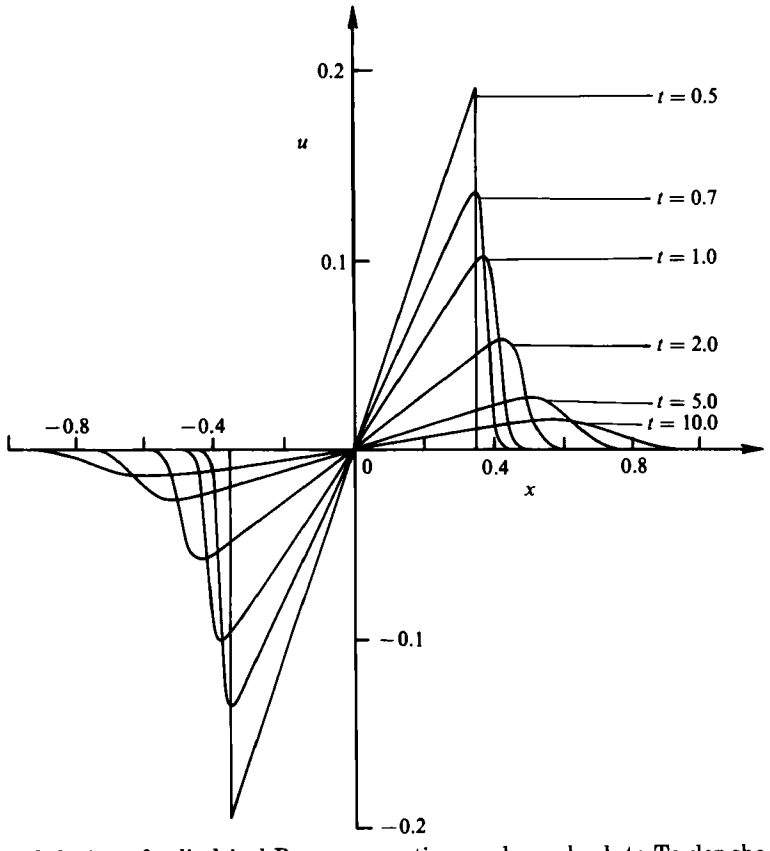

FIGURE 3. Solution of cylindrical Burgers equation: embryo shock to Taylor shock.

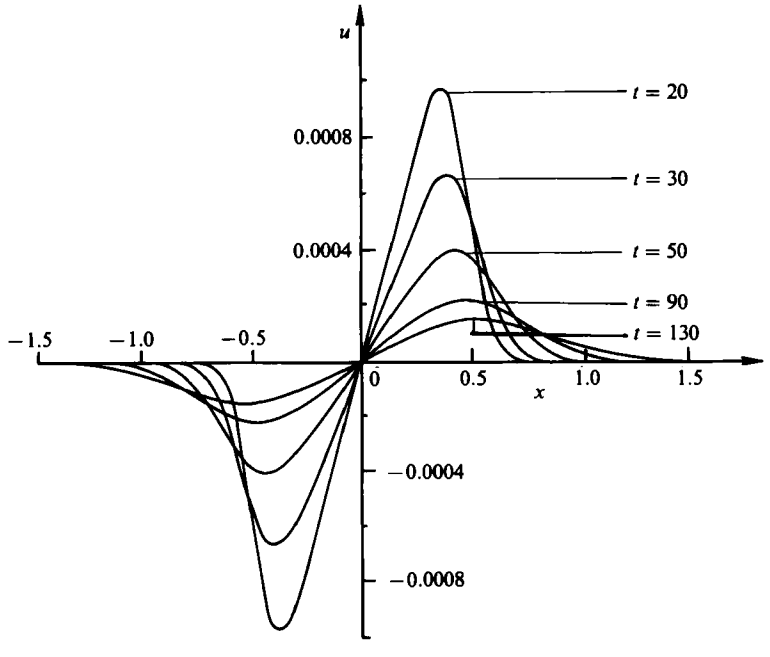

FIGURE 4. Solution of cylindrical Burgers equation: thick-shock regime.

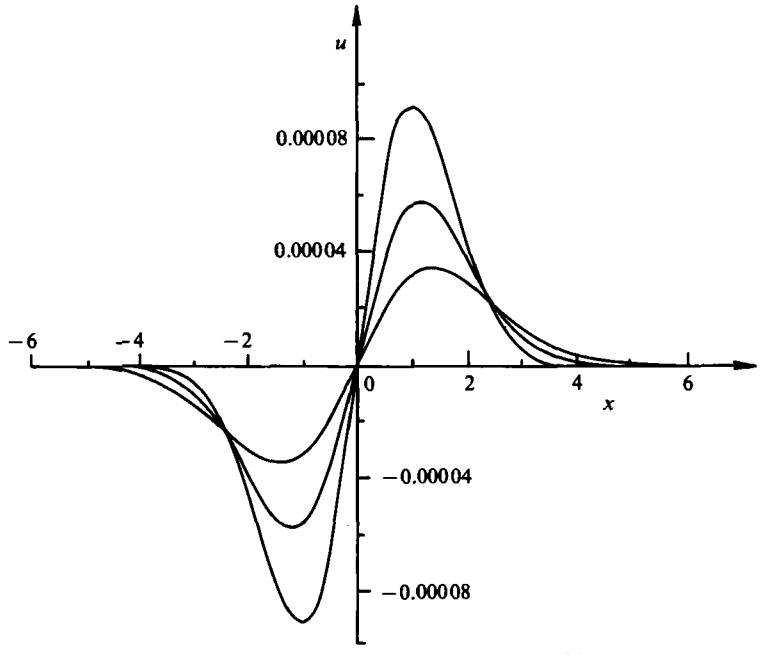

FIGURE 5. Solution of cylindrical Burgers equation: old-age regime.

of the profile at $x = 0$ and that given by the inviscid solution, $u_x(0,t) = 1/(2t)$. These two slopes agree to three significant places up to $t \approx 100$. The numerical Reynolds number and that given by SS,

$$R = -\frac{1}{2} + \left(\frac{t_0}{t}\right)^{\frac{1}{2}}, \tag{6.3}$$

agree to 3 significant digits up to $t \approx 100$. Here t_0 is a constant of integration in the derivation of (6.3) from the cylindrical Burgers equation and was evaluated by SS using the initial Reynolds number in the Taylor-shock regime. After $t \approx 100$, the disparity between the numerical Reynolds number and that obtained from (6.3) increases. Indeed, at $t \approx 1000$, (6.3) gives a negative Reynolds number! Thus, (6.3) is valid until $R \approx 1$. On the other hand, formula (5.18) gives the Reynolds number with an error less than 3.5% from $t \approx 300$ to $t \approx \infty$. The accuracy improves with time, confirming the asymptotic (with respect to time) nature of the solution (5.15). We note that the asymptotic solution is rendered unique by the choice of positive sign for $b_3^{\frac{1}{2}}$. We must, however, point out that the solution has been found up to only three terms in the series for V. This is adequate for the purpose of finding the Reynolds number. The values of the constants b_3 and C in (5.18) were found by using the values of the Reynolds number at two distant times, $t = 500$ and $t = 1600$. They were found to be $b_3^{-\frac{1}{2}} = 26.44$ and $C^{\frac{1}{2}} = -4.716$. The old-age solution given by Leibovich & Seebass (1974) is

$$u = C_1 t^{-2} x \exp(-x^2/2\delta t). \tag{6.4}$$

The constant C_1, by comparison with the numerical solution (i.e. matching the analytic and numerical maxima), was found to be approximately 161.02. Table 9 shows the analytic and numerical values of u_m and Reynolds number in the old-age regime. The agreement is quite satisfactory.

	$10^4\, u_m$		Difference	Reynolds numbers	
t	Num.	Old age	(2)−(3)	Num.	Old age
(1)	(2)	(3)	(4)	(5)	(6)
1550	0.504	0.502	−0.002	0.1067	0.1067
1600	0.482	0.480	−0.002	0.1035	0.1034
1650	0.462	0.459	−0.003	0.1005	0.1002
1700	0.442	0.440	−0.002	0.0977	0.0972
1800	0.408	0.402	−0.006	0.0925	0.0919
1850	0.392	0.387	−0.005	0.0901	0.0890
1900	0.378	0.372	−0.006	0.0879	0.0871
1950	0.364	0.358	−0.006	0.0857	0.0848
2000	0.350	0.343	−0.007	0.0836	0.0827

TABLE 9. 'Old-age' solution for the cylindrical Burgers equation: numerical, and analytic according to (5.14) with $c_1 = 161.02$

We have compared the old-age solution of (2.8),

$$\bar{V} = C_s \frac{X}{\epsilon^2 T^3} \exp(-X^2/\epsilon T^2), \tag{6.5}$$

for the cylindrically symmetric case, ($g(T) = \frac{1}{2}(T + T_0 - 1)$ in (2.8)), with that obtained numerically. The initial profile was taken to be the discontinuous sawtooth (2.10). The parameters T_0 and ϵ (see (2.11)) were chosen to be 1.2 and 0.017, and the mesh sizes Δx and ΔT were selected to be 0.005 and 0.0001, respectively. The full initial N wave occupied 400 points. When the profile became smooth, the PS scheme was replaced by the IMP scheme. The mesh sizes Δx and ΔT were increased to 0.01 and 0.005, respectively, as the N wave broadened and had everywhere relatively small gradients. Unlike the solution of (1.3), the solution of (2.8) required the inversion of a very large order (about 1000–2500) matrix as the profile evolved from one with a Taylor shock to its old age. This required large computing time. The profile attains its old age at $T \approx 99$. The constant C_s in (6.5) is 0.34, and the maximum amplitude is $O(10^{-3})$. The maximum amplitude of the numerical solution in the entire old-age phase agrees very well with that from (6.5) with $C_s = 0.34$. However, the prediction of CS that C_s is independent of ϵ, cannot be checked from this single computation at one value of ϵ.

7. The spherical Burgers equation

The initial discontinuous profile for this case was taken to be

$$u(x, t_i) = \begin{cases} \dfrac{x}{t_i \ln t_i} & \text{for } |x| < d_0, \\ 0 & \text{for } |x| > d_0, \end{cases} \tag{7.1}$$

where $t_i = 1.76$, $d_0 = 0.2$, and $R(t_i) = 20$. This profile evolves through the embryonic-shock stage to one with a Taylor shock as shown in figure 6. Table 10 shows the shock details in the manner discussed earlier for the cylindrical case. The CS formula for the shock centre

$$s = d_0 T^{\frac{1}{2}} \left(\frac{1 - \delta e^{-1/T_0} (E_i(T/T_0) - E_0(1/T_0))}{(\gamma + 1) U_0 d_0} \right), \tag{7.2}$$

where

$$E_i(x) = \int_{-\infty}^{x} t^{-1} \exp(t)\, dt \tag{7.3}$$

				Shock centre				
t	x_m	u_m	Shock width	Num.	CS	Difference (5)−(6)	u_d	u_d/u_m
(1)	(2)	(3)	(4)	(5)	(6)	(7)	(8)	(9)
2.0	0.204	0.144	0.028	0.225	0.225	0.0	0.012	0.086
3.0	0.245	0.072	0.049	0.285	0.289	−0.004	0.013	0.185
4.0	0.270	0.046	0.068	0.321	0.326	−0.005	0.009	0.196
5.0	0.284	0.033	0.085	0.347	0.351	−0.004	0.007	0.197
6.0	0.295	0.025	0.1	0.367	0.370	−0.003	0.005	0.2
7.0	0.302	0.02	0.114	0.385	0.385	0.0	0.004	0.205
8.0	0.308	0.017	0.128	0.399	0.398	0.001	0.004	0.21
9.0	0.312	0.014	0.141	0.412	0.408	0.004	0.003	0.232
10.0	0.316	0.012	0.153	0.424	0.417	0.007	0.003	0.253
15.0	0.328	0.007	0.205	0.470	0.448	0.022	0.002	0.322
20.0	0.335	0.005	0.249	0.505	0.467	0.038	0.002	0.354
30.0	0.345	0.002	0.32	0.560	0.488	0.072	0.001	0.406
50.0	0.363	0.001	0.428	0.644	0.506	0.138	0.0005	0.44
100.0	0.412	0.0004	0.611	0.806	0.506	0.299	0.0002	0.45
150.0	0.462	0.0002	0.742	0.936	0.488	0.448	0.0001	0.458

TABLE 10. Shock details for the spherical Burgers equation: $T_0 = 2.12$. $\epsilon = 0.0065$ (see (2.11)); abbreviations are explained in table 5

gives an accurate description of the Taylor shock up to $t \approx 16$, with an error of less than 5%. At this stage the shock width is $O(d_0)$. Figures 6–8 display the typical form of the N wave when it has a Taylor shock structure, when it has a thick shock, and when it has attained old age, respectively. The Reynolds number as given by the numerical solution SS, and the generalized similarity solution for the 'scaled' inverse of u are given in table 11. This table also gives $u_x(0,t)$ as obtained numerically and by the inviscid expression $1/(t \ln t)$. The agreement is very good up to $t \approx 30$, when the Reynolds number is about 1. The approximate formula of SS is

$$R = \frac{c}{t} - \frac{1}{2t}\int_{t_1}^{t} \frac{\mathrm{d}y}{\ln y}. \tag{7.4}$$

The disparity between (7.4) and the numerical Reynolds number increases until R, as given by (7.4), becomes negative at $t \approx 350$. Thus, the SS formula works again up to $R \approx 1$. The 'reasonable choice' of $f_0(t)$ in (5.25) gives a Reynolds number (5.26) which agrees very well with the numerical Reynolds number throughout the evolution of the profile, from $t = 3$ to $t = 900$. At this stage, that is, when $t = 900$, the profile practically dies out. The constants a_0 and $\bar{C}$ in (5.26) were found to be 0.0028 and 35.50, respectively. The maximum error is 2% at $t \approx 50$. The old-age formula

$$u = C_2 x t^{-5/2} \exp(-x^2/2\delta t), \tag{7.5}$$

with $C_2 = 263.92$ obtained from the numerical solution gives a satisfactory profile and Reynolds number, as shown in table 12. We also verified the old-age analytic solution of CS,

$$\bar{V} \sim \frac{1}{6\pi^{\frac{1}{2}}} T^{\frac{1}{2}} \frac{X}{(\epsilon T_0 \mathrm{e}^{T/T_0})^{\frac{3}{2}}} \exp\left(-\frac{X^2}{4\epsilon T_0 \mathrm{e}^{T/T_0}}\right), \tag{7.6}$$

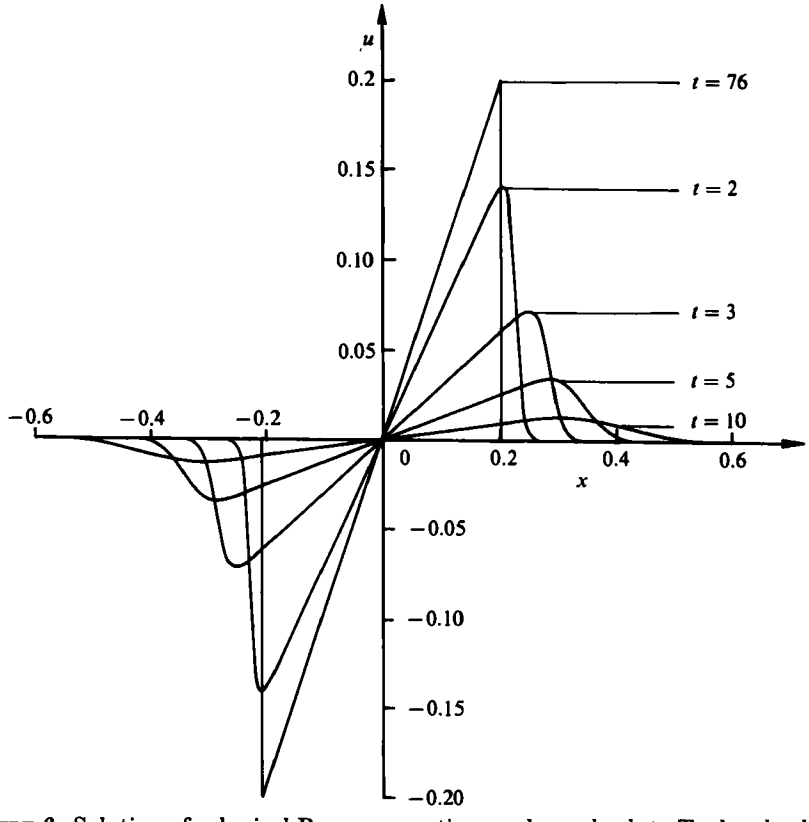

FIGURE 6. Solution of spherical Burgers equation: embryo shock to Taylor shock.

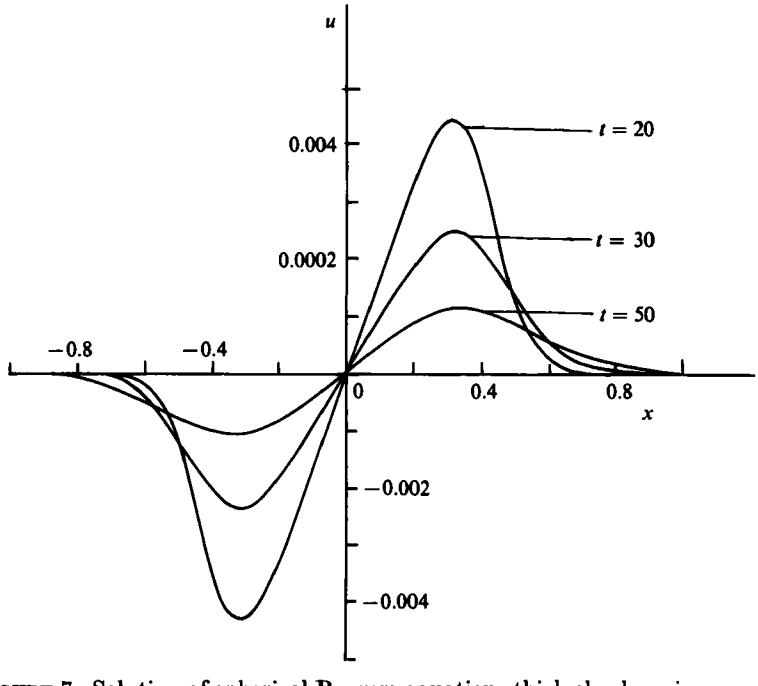

FIGURE 7. Solution of spherical Burgers equation: thick-shock regime.

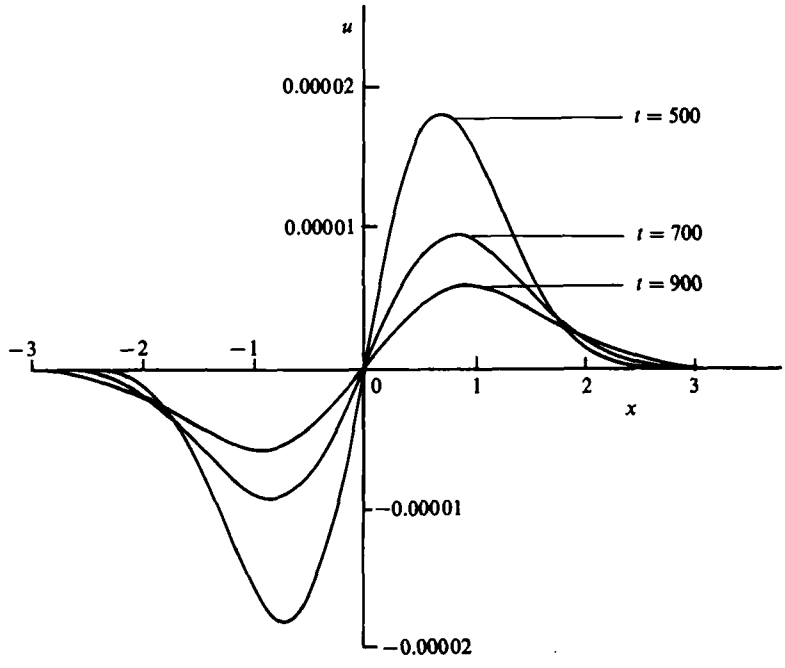

FIGURE 8. Solution of spherical Burgers equation: old-age regime.

	R			$u_x(0,t)$	
t	Num.	Equation (7.4)	Equation (5.26)	Num.	Analytic
5.0	6.95788	6.94885	6.95113	0.12442	0.12414
10.0	3.35331	3.34906	3.35361	0.04348	0.04341
15.0	2.16937	2.16666	2.17273	0.02463	0.02461
20.0	1.58335	1.58133	1.58876	0.01666	0.01669
30.0	1.00411	1.00233	1.01228	0.00961	0.00980
40.0	0.71909	0.71656	0.72888	0.00642	0.00678
50.0	0.55095	0.54697	0.56154	0.00461	0.00511
100.0	0.23003	0.21521	0.23932	0.00143	0.00217
150.0	0.13371	0.10889	0.14022	0.00065	0.00133
200.0	0.08992	0.05744	0.09428	0.00035	0.00094
250.0	0.06563	0.02747	0.06861	0.00022	0.00072
350.0	0.04047	−0.00546	0.04179	0.00010	0.00049
450.0	0.02808	−0.02281	0.02851	0.00005	0.00036
550.0	0.02090	−0.03331	0.02085	0.00003	0.00029
650.0	0.01628	−0.04023	0.01598	0.00002	0.00024
750.0	0.01311	−0.04505	0.01268	0.00001	0.00020
850.02	0.01083	−0.04857	0.01032	0.00001	0.00017
948.0	0.00914	−0.05116	0.00860	0.00001	0.00015

TABLE 11. Reynolds number for the spherical Burgers equation at different times: numerical, and analytic according to (7.4) and (5.26) with $\bar{c} = 35.50$ and $a_0 = 0.0028$. Numerical and analytic values of $u_x(0,t)$ are also shown

	$10^4\,u_m$		Difference	Reynolds numbers	
t	Num.	Old age	(2)−(3)	Num.	Old age
(1)	(2)	(3)	(4)	(5)	(6)
550	0.167	0.167	0.0	0.0204	0.0209
622	0.132	0.131	−0.001	0.0174	0.0174
650	0.121	0.120	−0.001	0.0163	0.0163
700	0.105	0.103	−0.002	0.0146	0.0146
750	0.092	0.090	−0.002	0.0131	0.0131
800	0.080	0.079	−0.002	0.0119	0.0119
850	0.072	0.070	−0.002	0.0108	0.0109
900	0.064	0.062	−0.002	0.0099	0.0100
948	0.058	0.056	−0.002	0.0091	0.0092

TABLE 12 'Old-age' solution for the spherical Burgers equation: numerical, and analytic according to (7.5) with $c_2 = 263.92$

(see (2.5)–(2.6) for notation). For the purpose, (2.8) was solved numerically. The parameters T_0 and ϵ were chosen to be 1.2 and 0.00431, respectively, and the time mesh size ΔT was taken to be 0.0001 initially. We found it expedient to solve (2.8) numerically because the exponential transformation which connects this equation with (1.2) would introduce considerable errors. Also, there is likely to be an inaccuracy in the manner in which the numerical solutions are matched with old-age solutions – either at the maxima or in the integral sense. The solution of (2.8) with variable viscosity attains its old age at $T \approx 11$, so the inaccuracy in the numerical solution will be relatively smaller in comparison with that for (1.2), for which the old age is attained at $t \approx 550$. The constant in the old-age solution is, therefore, more accurately obtained from the old-age solution of (2.8). The time constant T_2 which heralds the onset of old age is given by $\epsilon T_2^{-1} \exp(T_2/T_0) = 1$ (see (3.47) of CS) and is found to be approximately 9.2. At this time the shock width $\epsilon^{\frac{1}{2}} \exp(\frac{1}{2}T_2/T_0)$ agrees closely with the scale $T_2^{\frac{1}{2}}$ of the main N wave, its magnitude being 3.0331 at $T = T_2 = 9.2$ (see above (3.47) of CS). The old age sets in at $T \approx 11$, when the maximum amplitude is $O(3 \times 10^{-3})$. The numerical solution at later times agrees with (7.6) very closely (to six decimal places). The order symbol in (7.6) becomes an equality if a factor 0.67 multiples the right-hand side. These calculations show that the evolutionary-shock regime prevails over a very restricted time range and is followed almost immediately by the old-age decay. Note, however, that this computation involves only a single value of ϵ and therefore cannot be regarded as confirming the ϵ-dependence predicted in (7.6).

8. Conclusions

The GBEs that appear in applications unfortunately do not lend themselves to exact analytic treatment. No 'Hopf–Cole-like' transformation is available to render them linear. One has therefore to take recourse to matched asymptotic analysis, generalized similarity analysis, etc., to cover at least some of the space and time domains. The complete solution of the problem starting from, say, a discontinuous initial N wave (or any other profile), is possible only by numerical methods. This is what we claim to have accomplished for the non-planar GBEs (see figures 9–10 for

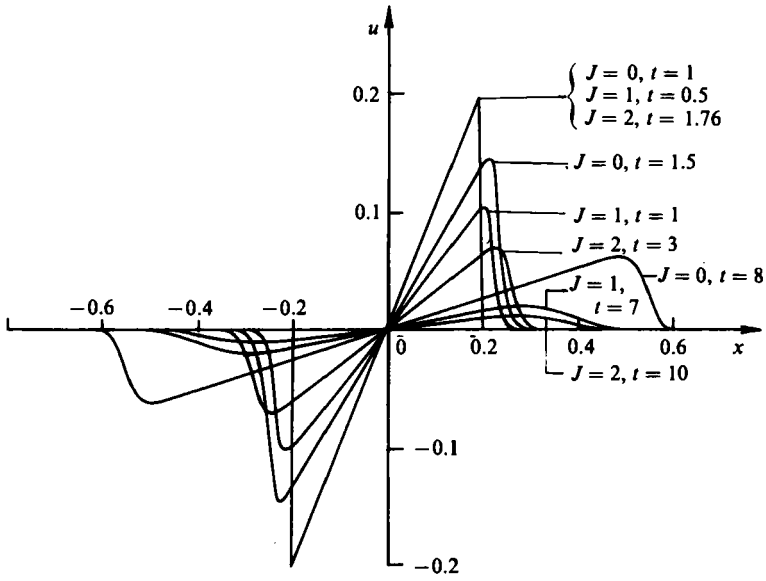

FIGURE 9. Solution of plane, cylindrical and spherical Burgers equations: from discontinuous initial profile to Taylor shock.

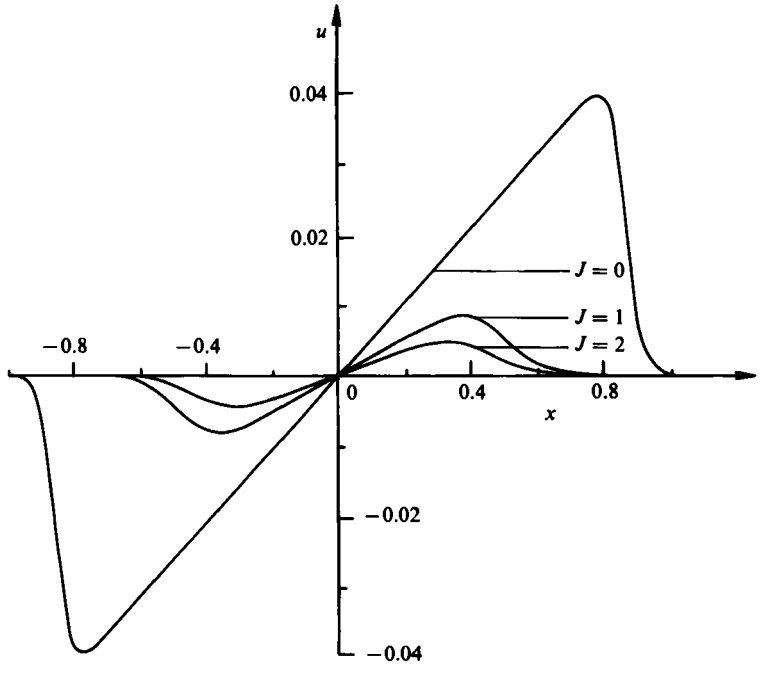

FIGURE 10. Solution of plane, cylindrical and spherical Burgers equation at $t = 20$.

the comparative evolution of the three N waves). We have ensured that the numerical solution is accurate in the entire time domain from the initial sawtooth form to the final old age of the solution. The pseudospectral finite difference method provided the necessary accuracy in the early part of the evolution of the wave profile when the shock is very steep and the implicit scheme is unable to tackle the sharp gradients. At later times when the shock has assumed a Taylor structure, the implicit scheme is sufficiently accurate and yields good results with a much smaller computational cost than the pseudospectral approach. The present problem poses most of the difficulties that a GBE can present and, therefore, the numerical methods given here are sufficiently sophisticated to handle any GBE. Even an initial-boundary-value problem should be easily amenable to the numerical methods used here.

By way of analysis, we have given a generalized similarity solution for the inverse function (see (5.3)) for $J = 1$, which extends the validity of the (linear) old-age solution (which may be referred to as the similarity solution in the present case) backward in time to a considerable span. This solution has been verified numerically and gives accurate Reynolds number over a long time. Our analysis for $J = 1$ covers time regimes over which the matched asymptotic solution of Crighton & Scott does not hold and, thus, supplements their results. On the other hand, Crighton & Scott (1979) have solved the spherically symmetric case for almost the entire evolution of the wave; there is a small space–time region over which an irreducible nonlinear problem remained unsolved. The order of the constant in the old-age solution was correctly found; however, the constant in the old-age solution for the cylindrically symmetric case could not be determined. We have supplemented these results especially for the cylindrically symmetric case, both numerically and analytically. Yet there are some analytic gaps which are not filled by either work. A complete exact analytic solution of this class of problems does not seem possible at this stage. We have checked our numerical solution with the analytic solution wherever they are available – the matched asymptotic solution, generalized similarity solution for the inverse function and the old-age solution – and have found good agreement among them. In particular, we have found the unknown numerical constants for the (dipole) old-age solutions by comparison with the numerical solution. For this purpose, we found it desirable to solve the form (2.8) of (2.3), which has a variable (time-dependent) coefficient of viscosity. This equation presents some difficulties of its own in its numerical solution (see §§6 and 7), but has the advantage that the old age is attained at a relatively shorter time in the variable T so that the errors of computation are small and the constants in the asymptotic formula (7.6) can be accurately determined. In turn the old-age solution verifies the veracity of the final stage of the numerical solution and confirms that no (serious) cumulative errors have been permitted by the numerical method (see tables 9 and 12) even though computation of the solution had to be carried out over a long time.

The authors are grateful to Professor Sir James Lighthill for his encouragement. They wish to express their sincere thanks to Professor D. G. Crighton for his constructive criticism and helpful suggestions.

REFERENCES

BENTON, E. R. & PLATZMAN, G. W. 1972 A table of solutions of one dimensional Burgers equations. *Q. Appl. Maths.* **30**, 195–212.

CANOSA, J. 1973 On a nonlinear diffusion equation describing population growth. *IBM J. Res. Develop.* **17**, 307–313.

CRIGHTON, D. G. 1979 Model equations of nonlinear acoustics. *Ann. Rev. Fluid Mech.* **11**, 11–33.

CRIGHTON, D. G. & SCOTT, J. F. 1979 Asymptotic solutions of model equations in nonlinear acoustics. *Phil. Trans. R. Soc. Lond.* A**292**, 101–134.

DOUGLAS, J. & JONES, B. F. 1963 On predictor-corrector methods for nonlinear parabolic differential equations. *J. Soc. Ind. Appl. Maths.* **11**, 195–204.

FORNBERG, B. & WHITHAM, G. B. 1978 A numerical and theoretical study of certain nonlinear wave phenomena. *Phil. Trans. R. Soc. Lond.* **289**, 373–404.

GAZDAG, J. 1973 Numerical schemes based on accurate computation of space derivatives. *J. Comp. Phys.* **13**, 100–113.

GAZDAG, J. & CANOSA, J. 1974 Numerical solution of Fisher's equation. *J. Appl. Prob.* **11**, 445–457.

LEIBOVICH, S. & SEEBASS, A. R. (eds) 1974 *Nonlinear Waves.* Cornell University Press.

LIGHTHILL, M. J. 1956 Viscosity effects in sound waves of finite amplitude. In *Surveys in Mechanics* (ed. G. K. Batchelor & R. M. Davies). Cambridge University Press.

SACHDEV, P. L. SEEBASS, A. R. 1973 Propagation of spherical and cylindrical N waves. *J. Fluid Mech.* **58**, 197–205.

SINAI, Y. L. 1976 Similarity solution of the axisymmetric Burgers equation. *Phys. Fluids* **19**, 1059–1060.

WHITHAM, G. B. 1974 *Linear and Nonlinear Waves.* Wiley Interscience.